

Bolometric detection of coherent Josephson coupling in a highly dissipative environment

Diego Subero,^{1,*} Olivier Maillet,^{1,2,†} Dmitry S. Golubev,¹ George Thomas,¹ Joonas T. Peltonen,¹ Bayan Karimi,^{1,3} Marco Marín-Suárez,¹ Alfredo Levy Yeyati,⁴ Rafael Sánchez,⁴ Sunghun Park,⁴ and Jukka P. Pekola¹

¹*PICO Group, QTF Centre of Excellence, Department of Applied Physics, Aalto University School of Science, P.O. Box 13500, 0076 Aalto, Finland*

²*Université Paris-Saclay, CEA, CNRS, SPEC, 91191 Gif-sur-Yvette, France*

³*QTF Centre of Excellence, Department of Physics,*

Faculty of Science, University of Helsinki, 00014 Helsinki, Finland

⁴*Departamento de Física Teórica de la Materia Condensada,*

Condensed Matter Physics Center (IFIMAC) and Instituto Nicolás Cabrera, Universidad Autónoma de Madrid, 28049 Madrid, Spain

The Josephson junction is a building block of quantum circuits. Its behavior, well understood when treated as an isolated entity, is strongly affected by coupling to an electromagnetic environment. In 1983 Schmid predicted that a Josephson junction shunted by a resistance exceeding the resistance quantum $R_Q = h/4e^2 \approx 6.45 \text{ k}\Omega$ for Cooper pairs would become insulating since the phase fluctuations would destroy the coherent Josephson coupling. Although this prediction has been confirmed in charge transport experiments, recent microwave measurements have questioned this interpretation. Here, we insert a small junction in a Johnson-Nyquist type setup, where it is driven by weak current noise arising from thermal fluctuations. Our heat probe minimally perturbs the junction's equilibrium, shedding light on features not visible in charge transport. We find that while charge transport through the junction is dissipative as expected, thermal transport is determined by the inductive-like Josephson response, unambiguously demonstrating that a supercurrent survives even deep into the expected insulating regime. The discrepancy between these two measurements highlights the difference between the low frequency and the high frequency response of a junction and calls for further theoretical and experimental inputs on the dynamics of Josephson junctions in a highly dissipative environment.

Thermal transport by photons in electrical circuits arises from Johnson-Nyquist noise [1, 2] between two resistive elements at unequal temperatures. The resulting current noise flowing in the ideally lossless circuit linking the two resistors provides an efficient channel for thermalization and energy exchange at very low temperatures [3, 4]. This current noise can be modulated by adding a suitable tunable dissipationless element in the circuit, which can conveniently be implemented by a magnetically [4–6] or electrically [7] controlled Josephson device. So far, both theoretical [8, 9] and experimental

approaches [4–7] of photonic heat transport had only considered on-chip resistors with resistance R much smaller than the superconducting resistance quantum R_Q , where the environmental back-action effect on the junctions is weak. More fundamentally, energy transport through quantum coherent systems strongly coupled to a dissipative environment, characterized by a large effective fine structure constant R/R_Q [10], remains largely unexplored [11].

It is well-established that the electrical transport properties of a superconducting junction depend on the electromagnetic environment in which it is embedded. Charge transport through a tunnel junction in an Ohmic environment with resistance comparable to the resistance quantum is suppressed at low voltage bias and temperature because of Coulomb blockade [12], and the extension of this phenomenon to superconducting junctions, which are intrinsically phase-coherent, comes naturally [12–15]. Recent experiments using this effect include the production of antibunched photons at high rates [16] and the suppression of the Andreev bound state-induced zero bias anomaly, which could be beneficial in the arduous search for Majorana quasiparticles [17]. For a Josephson junction shunted by a resistor with resistance exceeding R_Q , the supercurrent peak (i.e., current at zero applied voltage bias) is predicted to disappear, being shifted to finite voltage as a result of inelastic Cooper pair tunneling [12]. This is accompanied by a sublinear current-voltage characteristic at low voltages, which signals an insulating behavior of the junction. This dissipative transition, which can be associated with the one predicted by Schmid [18] and Bulgadaev [19], was first confirmed in dc charge transport experiments [13, 15, 20]. However, recent admittance measurements of small junctions, shunted by a highly Ohmic environment [21] called into question the scenario of a dissipative phase transition, leading to further debate about the very existence of this transition [22–25].

In this context, we present a heat transport experiment in which a small tunable junction (effectively a superconducting quantum interference device SQUID) is

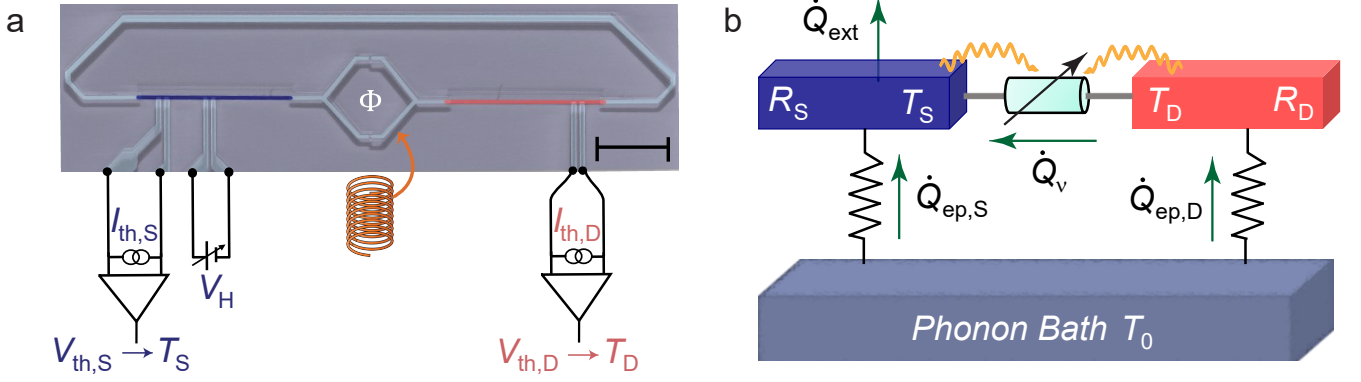


FIG. 1. a- Colored scanning electron micrograph (scale bar: $5\ \mu\text{m}$) highlighting the Cr normal metal (blue and red) and the aluminum superconducting leads (light blue). The Josephson energy of the SQUID is tuned with an external magnetic field. Aluminum leads (vertical, light blue) are connected through an oxide tunnel barrier to the Cr-strip to cool down its electrons locally or as an electronic temperature sensor using a floating dc current source. b.- Schematic illustration of the thermal model of the system. The drain-source heat flow \dot{Q}_v is adjusted by the SQUID. The source and drain electron baths are thermally coupled to the phonon bath (which here is hotter), receiving a power $\dot{Q}_{\text{ep},S}$ and $\dot{Q}_{\text{ep},D}$, respectively. Wiggly lines highlight the interaction between the SQUID and the Ohmic environment, mediated by photons.

embedded in a Johnson-Nyquist setup with hot and cold resistances $> R_Q$ to explore this regime. The SQUID geometry enables magnetic-flux control of the photonic heat current [4]. It is intended to demonstrate the destruction or resilience of the Josephson coupling through the observations of heat flow oscillations, or lack thereof if the junctions are truly insulating. We find that the magnitude of heat current flowing from one resistor to another remains close to the value given by the quantum limit, and it exhibits clear oscillations with the external magnetic flux, similarly to the systems embedded in a low impedance environment [4]. While this observation might point towards a survival of the dc Josephson current effect, a control experiment on dc charge transport shows clear suppression of the charge current at low bias caused by the environmental Coulomb blockade, as reported in earlier experiments [13, 20]. This apparent contradiction, highlighting the role of heat transport as a complementary probe when many-body correlations are present [26, 27], is discussed within the existing theoretical and experimental literature.

Our device (see Fig. 1a for an SEM image) consists of a SQUID between two nominally identical on-chip thin chromium resistors acting as thermal baths, from now on referred to as a source and drain with resistance R_S and R_D , respectively. Each arm of the SQUID is galvanically connected to one source and drain resistor of volume $\Omega = 10 \times 0.1 \times 0.014\ \mu\text{m}^3$ and whose resistance is nominally equal to that of an independently measured resistor with same dimensions on the same chip, with a value $R_S = R_D = 11 \pm 0.5\ \text{k}\Omega$ (see Supplemental S1, Fig. S2). The distance between the SQUID and the resistors is kept short (a few microns) to avoid suppression of environment-induced effects via stray capacitance. The series configuration of the SQUID and resistors is fur-

ther closed into a loop by a superconducting line. This warrants efficient electromagnetic heat transport through improved impedance matching [28]. The clean contact between chromium and superconducting aluminum leads serves as an Andreev-mirror [29], which enables essentially perfect conversion to charge transport by Cooper pairs in the superconducting strips while effectively suppressing quasiparticle heat diffusion along them at low temperatures ($\lesssim 200\ \text{mK}$) [28]. Four external superconducting leads are contacted with the source resistor through a thin oxide barrier, forming NIS-tunnel junctions. A pair of these junctions is used to measure the electronic temperature (in the case of quasi-equilibrium where the electron temperature is well-defined [30]) by applying a small dc-current bias through it, whereas another pair is used to locally cool the resistor when voltage-biased [30]. The electron temperature of the drain resistor is measured simultaneously by another SI-NIS junction structure, as depicted in Fig. 1a. We have presented data on two samples, henceforth called Sample I and Sample II.

We first measure the current-voltage characteristics (IVC) of a reference sample (see Fig. 2a) on the same chip from now on called “Replica”, with nominally equal parameters as the main sample. This provides estimates of parameters for the heat transport experiments and enables comparison between charge and heat transport behavior. Figure 2b and 2c show the IVC for two Replica samples at a phonon temperature of $T_0 = 87\ \text{mK}$ in the low bias region at two different magnetic flux values $\Phi = 0$ (solid circles) and $\Phi = \Phi_0/2$ (open circles) with $\Phi_0 = \pi\hbar/e$ the superconducting magnetic flux quantum. Suppression, with respect to the unblocked case, is observed in the low-bias dc current through the SQUID, which is more robust for Replica II (panel c) due to its

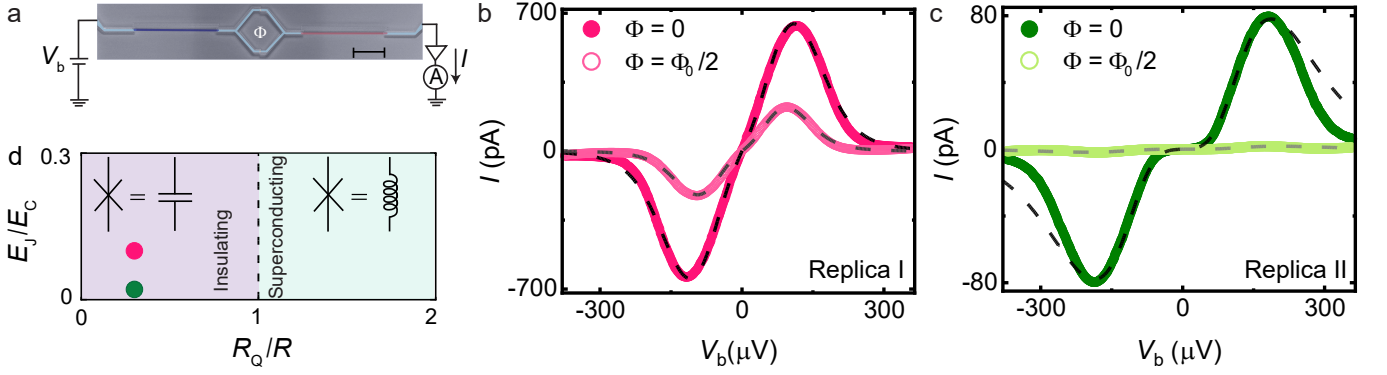


FIG. 2. a.- Scanning electron micrograph of one of the Replica samples (scale bar: $5 \mu\text{m}$) with the schematics of the IV measurement. b, c.- A close-up of the IVC at the low-bias voltage for Replica I and Replica II samples measured at a cryostat temperature of 87 mK exhibiting the Coulomb blockade feature. The measurements were recorded at two magnetic flux values $\Phi = 0$ (solid circles) and $\Phi = \Phi_0/2$ (open circles). The dashed lines are the theoretical results obtained by the standard $P(E)$ -theory for two magnetic flux values, $\Phi = 0$ (dashed black line) and $\Phi = \Phi_0/2$ (dashed gray line). The fit parameters for Replica I of panel b are: critical current $I_C = 7.9 \text{ nA}$, Josephson energy $E_J \sim 0.19 \text{ K}$, charging energy $E_C \sim 0.8 \text{ K}$ and, for Replica II of panel c: $I_C = 3.3 \text{ nA}$, $E_J \sim 0.08 \text{ K}$, $E_C = 1.4 \text{ K}$. The resistance of Cr-strips is $R_e = 11 \text{ k}\Omega$ for both samples. d.- Illustration of the Schmid phase diagram for a Josephson junction attached to a resistive environment R at zero temperature. Here, $R = R_S + R_D = 2R_e$ is the total resistance of the environment. Our samples are well placed in the insulating part, represented by the two points.

higher charging energy E_C . This observation is well understood in the framework of dynamical Coulomb blockade [12]: the resistive environment impedes charge relaxation after a Cooper-pair tunneling event through junctions with high charging energy, which translates to a conductance reduction at low energy [12]. The magnitude of E_C (0.8 K for Replica I and 1.4 K for Replica II) is extracted from the current peak feature appearing in the IVC, which for small Josephson junctions in contact with an environment impedance with $R \gg R_Q$ occurs at a voltage bias $eV_b \sim 2E_C$ [13, 31]. The Josephson energy is estimated by using the Ambegaokar-Baratoff relation as $E_J = \Phi_0 \Delta / 4eR_J$ (0.07 K for Replica I and 0.03 K for Replica II), with $\Delta \approx 200 \mu\text{eV}$ the aluminum superconducting energy gap and R_J the quasiparticle tunnel resistance of the SQUID. The dashed lines in Fig. 2b and 2c are the theoretical results obtained by the standard $P(E)$ theory [12] in an RC environment, which highlights the effect of the electromagnetic environment on Josephson phase fluctuations (see Supplemental S2 for more details). In these calculations, we include overheating by the applied bias in good agreement with our data. The data at $\Phi = \Phi_0/2$ for Replica I is fitted by considering an asymmetry factor on the SQUID critical current of $d = 0.54$ (see Supplemental S2). Note that the critical current I_C was used as a fitting parameter in the model. Finally, Fig. 2d shows the Schmid phase diagram with the two points related to each Replica sample, showing their insulating character as expected.

With these results as a reference, we now turn to heat transport measurements, the main focus of this work. The power flowing from drain to source \dot{Q}_ν under a thermal gradient is determined by measuring the electronic

temperatures of the drain T_D and the source T_S . The temperature difference is generated by dc biasing the source resistor with a voltage $V_H \lesssim 2\Delta/e$ that enables electronic cooling of the source by removal of hot electrons [28, 30], as depicted in Fig. 3a and 3b. In steady-state, these temperatures involve the different energy relaxation channels in the system, as illustrated in the thermal model that accounts for our setup shown in Fig. 1b. By continuity (valid below 200 mK, when quasiparticle heat diffusion along the superconductor can be neglected [28]) a direct relation between \dot{Q}_ν and the temperatures (T_S, T_D, T_0) measured in the system is found

$$\dot{Q}_\nu(T_S, T_D, \Phi) = \dot{Q}_{\text{ep,D}}(T_D, T_0), \quad (1)$$

where $\dot{Q}_{\text{ep,D}} = \Sigma \Omega [T_D^6 - T_0^6]$ is the electron-phonon heat current governed by the drain resistor. Here, Σ is the electron-phonon coupling constant of the normal metal which was measured independently to be $\Sigma = (12 \pm 0.25) \times 10^9 \text{ WK}^{-6}\text{m}^{-3}$ (unpublished). With our experimental setup (see Fig. 1a), we have full control of all temperatures and, therefore, the powers involved in the system, leading to an accurate and fully calibrated measurement of the thermal conductance between the drain and source.

Figure 3c and 3d show the temperature drops $\Delta T_i = T_i(V_H^{\text{opt}}) - T_i(V_H = 0)$, $i = S, D$ at the optimum cooling bias of the SINIS $V_H^{\text{opt}} \lesssim 2\Delta/e$, for the two samples at two magnetic flux values. At $V_H = 0$ the electronic temperature equals the phonon temperature T_0 . These drops characterize the thermal coupling between the drain and source, i.e., the thermal conduc-

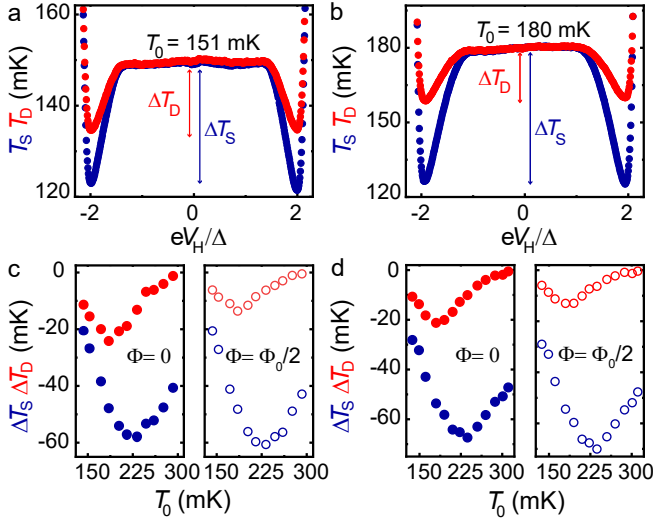


FIG. 3. a, b.- Electronic temperature of the source T_S (blue points) and drain T_D resistor (red points) at $\Phi = 0$ for Sample I and Sample II, respectively, as a function of the bias voltage recorded at phonon temperature T_0 of 151 mK (Sample I) and 180 mK (Sample II). c, d.- Temperature drops ΔT_S (blue circles) and ΔT_D (red circles) recorded at two magnetic flux values $\Phi = 0$ (solid circles) and $\Phi = \Phi_0/2$ (open circles) measured at different values of T_0 .

tance from drain to source. Source and drain temperature drops differ for the two magnetic fluxes supplied. At $\Phi = \Phi_0/2$, a significant reduction of the electronic temperature drop in the drain resistor is observed, indicating that the photonic channel effectively dominates the transport mechanism at lower temperatures. The significant flux-tunability of the remote cooling process is a characteristic feature of SQUID interference [4], which suggests that the Josephson coupling is not destroyed by the environmental back-action. As T_0 increases above 200 mK, the photon thermal coupling gets smaller with respect to electron-phonon coupling.

To quantify the power transferred from the drain to the source resistor through a photon channel, the electronic temperatures measured on the two baths have been converted to heat current \dot{Q}_ν by using Eq. (1) and compared with the maximum power that can be transmitted through a single ballistic channel given by $\dot{Q}_Q = \frac{\pi k_B^2}{12\hbar}(T_D^2 - T_S^2)$ [32]. The photonic heat current for the two samples in the temperature range of 150-200 mK is shown in Figs. 4a and 4b. For Sample I at $\Phi = 0$ (solid circles), the energy is transferred from the drain to the source at a rate very close to that dictated by the quantum of thermal conductance (black line). Nevertheless, a minor deviation of \dot{Q}_ν from the quantum limit prediction is seen for Sample II. As soon as the magnetic flux increases near the half flux quantum $\Phi = \Phi_0/2$ (empty circles), the heat current \dot{Q}_ν for both samples tends to decrease due to weaker photonic coupling.

We then confront the data with theoretical calculations based on the Landauer relation for heat current from drain to source [3],

$$\dot{Q}_\nu = \int_0^\infty \frac{d\omega}{2\pi} \hbar \omega \tau(\omega, \Phi) \left[\frac{1}{e^{\hbar\omega/k_B T_D} - 1} - \frac{1}{e^{\hbar\omega/k_B T_S} - 1} \right], \quad (2)$$

where $\tau(\omega, \Phi)$ is the transmission probability of the thermal radiation from the drain to the source at angular frequency ω . In the limit of small phase fluctuations around a given average phase bias φ , the SQUID can conveniently be approximated by a harmonic oscillator. In electrical terms, this translates to an effective phase-dependent Josephson inductance $L_{\text{eff}}(\Phi) = \hbar/(2e|I_c(\Phi)|\langle\cos\varphi\rangle)$ in parallel with a capacitance (see Fig. 4e), where $\langle\cos\varphi\rangle$ is an average over phase fluctuations [24, 33]. Within this linear model, and by assuming the lumped approximation (valid since the dominant radiation wavelength $\lambda_{\text{th}} = hc/k_B T \sim 10$ cm at 150 mK is much larger than the circuit characteristic dimensions ~ 50 μm), the power transmission coefficient can be explicitly written [3, 9] as $\tau(\omega, \Phi) = 4R_S R_D / |Z_T(\omega, \Phi)|^2$ (see methods), with $Z_T(\omega, \Phi)$ the frequency-dependent total series impedance of the circuit. In this framework, the maximum heat transfer is expected for a perfect impedance matching when $R_S = R_D$ and when the phase fluctuations are small, i.e., $\langle\cos\varphi\rangle \simeq 1$ under no net electrical bias. However, for strong phase fluctuations at high resistances $R_S + R_D > R_Q$, one naively expects the average value of the cosine to almost vanish, $\langle\cos\varphi\rangle \approx 0$. Indeed, we have shown above that the dc charge transport measurements of the Replica samples are well described by the usual $P(E)$ theory of Coulomb blockade, which implies $\langle\cos\varphi\rangle \approx 0$. Assuming this, the SQUID can be regarded as a parallel connection of a capacitor C_J and of high effective impedance $\tilde{Z}(\omega, \Phi) \propto 1/I_c^2(\Phi)$, see Fig. 4f. Then the modulation of the Josephson coupling by flux almost does not affect the transmission probability $\tau(\omega, \Phi)$, and the oscillations of the heat flow are expected to be very small. Below we will show that the strong modulation of the heat flux observed in our experiment is consistent with the assumption of nonvanishing $\langle\cos\varphi\rangle$ rather than with $\langle\cos\varphi\rangle \approx 0$.

The dashed lines displayed in figures 4a and 4b are the theoretical results of \dot{Q}_ν obtained within the linear model for the corresponding magnetic fluxes applied. For Sample I, reasonable agreement with the experimental data at $\Phi = 0$ is found if we use the bare Josephson junction inductance in the calculated Z_T . Nevertheless, for Sample II, a significant deviation from the data is observed as the temperature is lowered. This deviation can be captured if we set the re-normalization parameter $\langle\cos\varphi\rangle = 0.18$. These results indicate that the photonic heat exchange from the drain to the source at lower thermal frequencies is mainly transmitted through the Josephson induc-

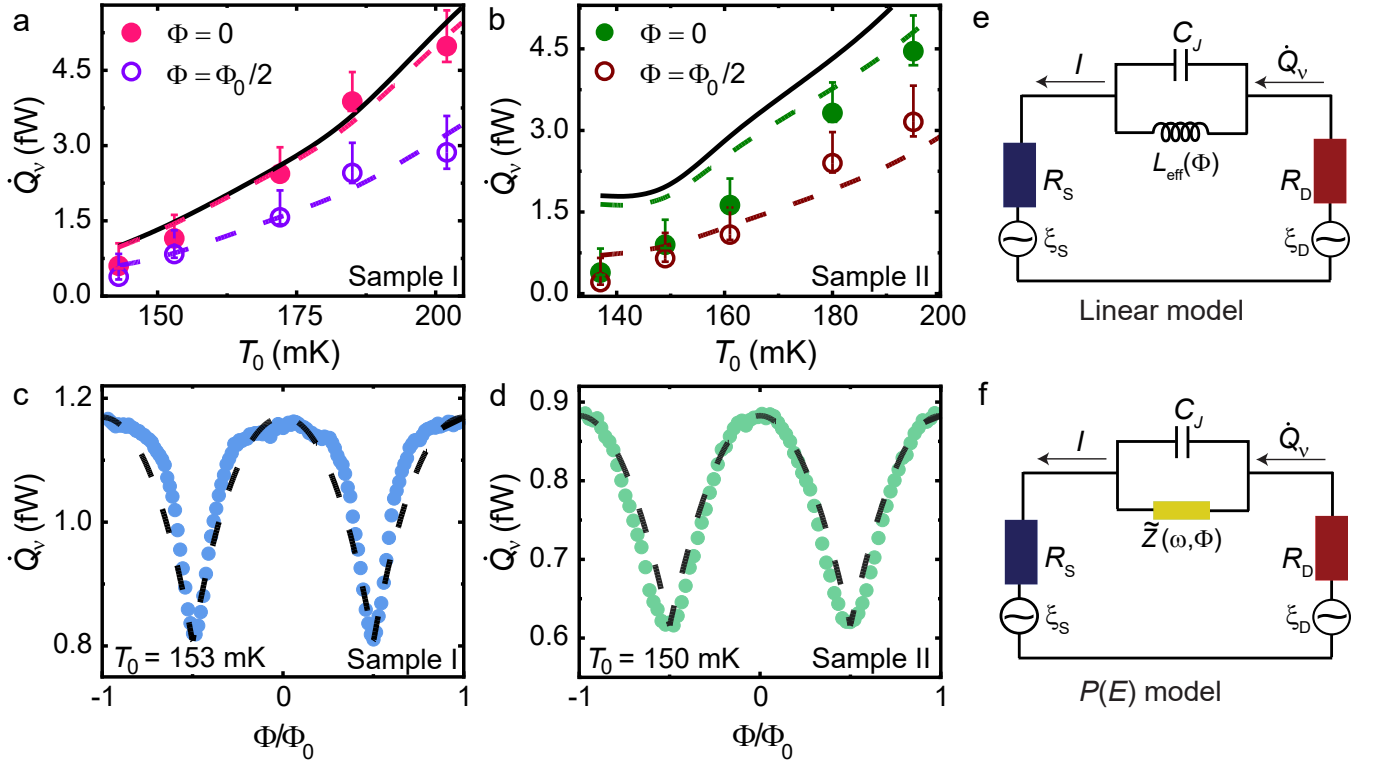


FIG. 4. a, b.- Photonic heat current from the drain to the source by using the continuity equation (1). The error bars are given in their lower and upper parts, the combination of the thermometer calibration and electron-phonon coupling constant uncertainties, while the upper part also includes the parasitic heat leak on the resistors due to the NIS junctions, with a 0.4 fW upper bound estimate. The solid line represents the power transmitted through a single channel at the quantum limit \dot{Q}_Q (see text). The dashed lines are the theoretical results obtained by solving Eq. (2) with a photon transmission probability computed within the linear circuit model, with the circuit parameters obtained from fitting the IVC of the Replica samples in Fig. 2. c, d.- Heat current modulation as a function of the reduced magnetic flux Φ/Φ_0 through the SQUID at a given temperature T_0 . The dashed lines are the theoretical results by setting $\langle \cos \varphi \rangle = 0.23$ for Sample I and $\langle \cos \varphi \rangle = 0.18$ for Sample II, keeping the same circuit parameters as in a and b. e.- Electric representation of the device in the linear model where the SQUID is approximated by a re-normalized variable inductor $L_{\text{eff}}(\Phi)$ in parallel with the junction geometric capacitor C_J , and f.- $P(E)$ model with an effective impedance $\tilde{Z}(\omega, \Phi)$ replacing the Josephson element.

tor channel. At $\Phi = \Phi_0/2$ (dashed purple and dark red lines), the power is reduced as expected, in fair agreement with the data. In this regime, the Josephson critical current is vanishingly small (making the inductance essentially infinite at the relevant frequencies); consequently, the power transmitted from the drain to the source takes place mainly through the junction capacitance C_J , which acts as a high-pass filter in the transmission and thus only enables a small fraction of the thermal fluctuations to be transmitted as current in the circuit. Furthermore, the heat current calculated within the $P(E)$ theory at $\Phi = 0$ shows a decrease of \dot{Q}_v to the level of the power obtained in the linear model at $\Phi = \Phi_0/2$ (see Supplemental Figs. S3b and S3c).

Figure 4c and Fig. 4d show the heat current modulations measured at given phonon temperatures T_0 for Sample I and Sample II, respectively. Clear oscillations with period Φ_0 are observed. This result unequivocally demonstrates that the inductive response of the junction

persists in the presence of strong environmental back-action, in contrast to what is observed for charge transport measurements in the Replica samples. The data is again compared to the theoretical models proposed. For simplicity, we have assumed a symmetric SQUID in the models. On the one hand, for the two examples presented, the heat current modulations are well captured with the linear model if we use a value of $\langle \cos \varphi \rangle = 0.23$ and $\langle \cos \varphi \rangle = 0.18$ for Sample I and Sample II, respectively. Besides, to fit the data of Sample II at other temperatures, values of $\langle \cos \varphi \rangle$ in the range 0.3-0.6 are used. On the other hand, the oscillation amplitude predicted by $P(E)$ theory ($\langle \cos \varphi \rangle \approx 0$) is much smaller than the amplitudes observed (see Supplemental Figs. S3d and S3e).

Let us now focus on the discrepancy between charge and heat transport measurements. One obvious difference resides in the relevant frequency range: at zero frequency, $P(E)$ theory of Coulomb blockade describes inco-

herent Cooper pair tunneling through the junction, and the transition to an insulating state predicted by Schmid and Bulgadaev is observed as R becomes greater than R_Q . On the other hand, heat transport deals with non-zero frequency current fluctuations flowing through the junction at zero net voltage bias. This was considered previously [34] through an extension of the static version of $P(E)$ theory to finite frequency transport. The derivation relies on the hypothesis of very weak Josephson coupling, $2E_J \ll k_B T$, which is not perfectly satisfied for Sample I, unlike for Sample II, where the contrast is the strongest (as highlighted by the sharp Coulomb gap observed in charge transport, see Fig. 2c). Our data provide piece of evidence on the overall puzzle. In that respect, recent high-frequency measurements of a small Josephson junction in an engineered high impedance environment have revealed the inelastic nature of the scattering process of a photon off the junction [35]. The conceptual similarity between the setup considered there and ours suggests that the description of the junction as a renormalized inductor [33], while appealing and useful for a basic understanding, is too simplistic because the nonlinearities of the junctions are responsible for phase fluctuations. Nevertheless, our bolometric technique enables to collect energy over a bandwidth $\sim k_B T/\hbar$ and, therefore, would not distinguish between several down-converted photons out of an inelastic process or a single elastically scattered photon.

In summary, we have experimentally demonstrated through heat transport measurements that a Josephson junction acts as an inductor even in the presence of a highly resistive environment. Though the interpretation of the dissipative transition can be debated [21, 24], the discrepancy between the heat transport measurements and the control charge transport measurements by us here and in the previous works [13, 20, 36], cannot be accounted for by the existing theory, and calls for further developments, both experimental and theoretical. Our findings are important not only from the fundamental physics point of view but also for future applications such as microbolometers or heat sink designs in quantum circuits. On a practical side, we note that any design aiming at increasing resistances for improved, quantum-limited tunable remote electronic cooling [4, 28] is much less sensitive to back-action effects than initially anticipated.

* diego.suberorengel@aalto.fi

† olivier.maillet@cea.fr

- [1] Nyquist, H. Thermal agitation of electric charge in conductors. *Phys. Rev.* **32**, 110 (1928).
- [2] Johnson, J. B. Thermal agitation of electricity in conductors. *Phys. Rev.* **32**, 97 (1928).
- [3] Schmidt, D. R., Schoelkopf, R. J. & Cleland, A. N. Photon-mediated thermal relaxation of electrons in nanostructures. *Phys. Rev. Lett.* **93**, 045901 (2004).
- [4] Meschke, M., Guichard, W. & Pekola, J. P. Single-mode heat conduction by photons. *Nature*. **444**, 187–190 (2006).
- [5] Partanen, M. *et al.* Flux-tunable heat sink for quantum electric circuits. *Sci. Rep.* **8**, 1–9 (2018).
- [6] Ronzani, A. *et al.* Tunable photonic heat transport in a quantum heat valve. *Nat. Phys.* **14**, 991–995 (2018).
- [7] Maillot, O. *et al.* Electric field control of radiative heat transfer in a superconducting circuit. *Nat. Commun.* **11**, 1–6 (2020).
- [8] Ojanen, T. & Jauho, A.-P. Mesoscopic photon heat transistor. *Phys. Rev. Lett.* **100**, 155902 (2008).
- [9] Pascal, L. M. A, Courtois, H. & Hekking, F. W. J. Circuit approach to photonic heat transport. *Phys. Rev. B.* **83**, 125113 (2011).
- [10] Kuzmin, R. *et al.* Quantum electrodynamics of a superconductor-insulator phase transition. *Nat. Phys.* **15**, 930–934 (2019).
- [11] Thomas, G., Pekola, J. P. & Golubev, D. S. Photonic heat transport across a Josephson junction. *Phys. Rev. B.* **100**, 094508 (2019).
- [12] Ingold, G.-L. & Nazarov, Y. V. Charge tunneling rates in ultrasmall junctions. (Springer) 21–107 (1992).
- [13] Kuzmin, L. S. *et al.* Coulomb blockade and incoherent tunneling of Cooper pairs in ultrasmall junctions affected by strong quantum fluctuations. *Phys. Rev. Lett.* **67**, 1161 (1991).
- [14] Averin, D. V., Nazarov, Y. V. & Odintsov, A. A. Incoherent tunneling of the Cooper pairs and magnetic flux quanta in ultrasmall Josephson junctions. *Phys. B Condens. Matter.* **165**, 945–946 (1990).
- [15] Corlevi, S. *et al.* Phase-charge duality of a Josephson junction in a fluctuating electromagnetic environment. *Phys. Rev. Lett.* **97**, 096802 (2006).
- [16] Grimm, A. *et al.* Bright on-demand source of anti-bunched microwave photons based on inelastic Cooper pair tunneling. *Phys. Rev. X.* **9**, 021016 (2019).
- [17] Zhang, S. *et al.* Suppressing Andreev bound state zero bias peaks using a strongly dissipative lead. *Phys. Rev. Lett.* **128**, 076803 (2022).
- [18] Schmid, A. Diffusion and localization in a dissipative quantum system. *Phys. Rev. Lett.* **51**, 1506 (1983).
- [19] Bulgadaev, S. A. Phase diagram of a dissipative quantum system. *JETP Lett.* **39**, 264–267 (1984).
- [20] Penttilä, J. S. *et al.* “Superconductor-Insulator transition” in a single Josephson junction. *Phys. Rev. Lett.* **82**, 1004 (1999).
- [21] Murani, A. *et al.* Absence of a dissipative quantum phase transition in Josephson junctions. *Phys. Rev. X.* **10**, 021003 (2020).
- [22] Hakonen, P. J. & Sonin, E. B. Comment on “Absence of a Dissipative Quantum Phase Transition in Josephson Junctions”. *Phys. Rev. X.* **11**, 018001 (2020).
- [23] Murani, A. *et al.* Reply to “Comment on ‘Absence of a Dissipative Quantum Phase Transition in Josephson Junctions’ ”. *Phys. Rev. X.* **11**, 018002 (2021).
- [24] Masuki, K. *et al.* Absence versus Presence of Dissipative Quantum Phase Transition in Josephson Junctions. *Phys. Rev. Lett.* **129**, 087001 (2022).
- [25] S  pulcre, T., Florens, S. & Snyman, I. Comment on “Absence versus Presence of Dissipative Quantum Phase Transition in Josephson Junctions”. arXiv:2210.00742 ,

1–2 (2022).

- [26] Giazotto, F. & Martínez-Pérez, M. J. The Josephson heat interferometer. *Nature*. **492**, 401–405 (2012).
- [27] Sivre, E. *et al.* Heat Coulomb blockade of one ballistic channel. *Nat. Phys.* **14**, 145–148 (2018).
- [28] Timofeev, A. *et al.* Electronic refrigeration at the quantum limit. *Phys. Rev. Lett.* **102**, 200801 (2009).
- [29] Andreev, A. F. Thermal conductivity of the intermediate state of superconductors II. *Sov. Phys. JETP*. **20**, 1490 (1965).
- [30] Giazotto, F. *et al.* Opportunities for mesoscopies in thermometry and refrigeration: Physics and applications. *Rev. Mod. Phys.* **78**, 217 (2006).
- [31] Devoret, M. *et al.* Effect of the electromagnetic environment on the Coulomb blockade in ultrasmall tunnel junctions. *Phys. Rev. Lett.* **64**, 1824 (1990).
- [32] Pendry, J. Quantum limits to the flow of information and entropy. *J. Phys. A Math: Mathematical and General*. **16**, 2161 (1983).
- [33] Joyez, P. Self-consistent dynamics of a Josephson junction in the presence of an arbitrary environment. *Phys. Rev. Lett.* **110**, 217003 (2013).
- [34] Saira, O. P. *et al.* Dispersive Thermometry with a Josephson Junction Coupled to a Resonator. *Phys. Rev. Applied*. **6**, 024005 (2016).
- [35] kuzmin, R. *et al.* Inelastic Scattering of a Photon by a Quantum Phase Slip. *Phys. Rev. Lett.* **126**, 197701 (2021).
- [36] Herrero, C. P. & Zaikin, A. D. Superconductor-insulator quantum phase transition in a single Josephson junction. *Phys. Rev. B*. **65**, 104516 (2002).
- [37] Dolan, G. J. Offset masks for lift-off photoprocessing. *Appl. Phys. Lett.* **31**, 337–339 (1977).

ACKNOWLEDGEMENTS

We thank P. Joyez, C. Altimiras, T. Yamamoto, J. Ankerhold, and J. Stockburger for illuminating discussions. We thank funding from Academy of Finland grant 336810, the Spanish State Research Agency through Grant RYC-2016-20778, and the EU for FET-Open contract AndQC. D.S. and J.P.P. acknowledge the support from the innovation programme under the European Research Council (ERC) programme (grant agreement 742559). This research was achieved using Otaniemi Research Infrastructure for Micro and Nanotechnologies (OtaNano).

AUTHOR CONTRIBUTIONS

The experiment was conceived by D.S., O.M., and J.P.P. and carried out by D.S. with contribution from O.M. and technical support by J.T.P. Sample fabrication was made by D.S. The theoretical model for heat transport based on the $P(E)$ theory was proposed by D.S.G., and the simulations were performed by D.S. The data were analyzed, and the manuscript was written by D.S. with important contributions from all the authors.

COMPETING INTERESTS

The authors declare no competing interests.

METHODS

Device fabrication and measurement

The devices were fabricated on 4-inch silicon substrates covered by 300 nm of Si/SiO₂ in an electron beam lithography (EBL, Vistec EBPG500 + operating at 100 kV) using a Ge-based hard mask process and the conventional shadow evaporation technique [37]. The silicon wafer was coated with 400 nm layers of poly(methylmethacrylate-methacrylate acid) P(MMA-MAA) resist spun for 1 min at 5500 rpm and baked at 180 °C for 20 min, twice. Then, on top of it 22 nm Ge layer was deposited in an electron-beam evaporator, and right after, approximately 50 nm thick of PMMA was coated with spun at 2500 rpm for 1 min and baked at 160 °C for 1 min. The devices were patterned on the PMMA layer by using electron beam lithography, and afterward, it was developed using a mixture solution with a concentration of 1:3 of methyl-isobutyl-ketone+isopropanol (MIBK). This pattern is transferred to the Ge mask using reactive ion etching (RIE) with tetrafluoromethane CF₄ plasma. The undercut in the MMA resist was created by oxygen plasma in the same RIE chamber. The metallic parts were made in three evaporation steps: first, a 20 nm layer of Al is evaporated at an evaporation angle of -22° . Then, static oxidation *in-situ* with pressure around 3 mbar for 3 minutes is made. This step defines the superconducting finger used as a thermometer, heater, and branch of the SQUID. In the second step, a 20 nm layer of Al is evaporated at an angle of -7° , forming the SQUID and the clean superconducting contact. Finally, a 14 nm layer of Cr is evaporated at an angle of 24° comprising the thermal bath. The nominal loop area of the SQUID for the two samples was 25 μm^2 . The main difference between them lies in the overlap area of the Josephson junction (JJ), which for Sample I is nominally $130 \times 140 \text{ nm}^2$ and for Sample II is $85 \times 85 \text{ nm}^2$. The resist was lifted-off in acetone at 52 °C. Then, the sample is attached to a sample carrier to be electrically connected to it by Al wire bonds for being measured. The bonded sample is placed on a stage with a double brass enclosure that acts as a radiation shield. It is connected to the mixing chamber of a custom-made plastic dilution refrigerator with a base temperature of approximately 40 mK. Dc signals were applied through cryogenic signal lines filtered with lossy coaxial cables with 0-10 kHz bandwidth connected to the bonded sample through a room-temperature breakout box. In order to sweep the SQUID Josephson energy, a perpendicular magnetic field is supplied by applying dc current to an external superconducting magnet inserted

around the vacuum can. All the input signals were applied and read out using programmable sources and multimeters. Amplifying current and voltage output signal was accomplished using a room temperature low noise current amplifier Femto DDPCA-300 and voltage amplifier Femto DLVPA-100-F-D, respectively. The cryostat temperature is controlled by applying a voltage across the heater resistance attached to the mixing chamber. The calibration of thermometers was done by monitoring the voltage drop across the SINIS configuration (current biased $I_{\text{th}} = 15$ pA) at zero heating bias voltage while varying the cryostat temperature up to 500 mK [30].

Photon transmission coefficient

As mentioned in the main text, the transmission probability of the thermal radiation from the source and drain $\tau(\omega, \Phi)$ used is Eq. (2) has been calculated within the two models. In the linear model approximation, $\tau(\omega, \Phi)$ can be written as

$$\tau(\omega, \Phi) = \frac{4R_S R_D}{|Z_T(\omega, \Phi)|^2}, \quad (3)$$

with

$$Z_T(\omega, \Phi) = R_S + R_D + \frac{1}{-i\omega C_J + \frac{2\pi I_c}{-i\omega \Phi_0} \langle \cos \varphi \rangle}. \quad (4)$$

In the charge dominated regime ($E_C \gg k_B T_{S,D} \gg 2E_J$) and taking into account the effect of the environment resistors through $P(E)$ function, the transmission

probability $\tau(\omega, \Phi)$ for the system studied reads [11],

$$\tau(\omega, \Phi) = \frac{4R_S R_D}{\left| R_S + R_D + \frac{1}{-i\omega C_J + \tilde{Z}^{-1}(\omega, \Phi)} \right|^2} + \frac{\pi^2 I_c^2}{2e^2} [P_S(\omega) - P_S(-\omega)][P_D(\omega) - P_D(-\omega)], \quad (5)$$

where $\tilde{Z}(\omega, \Phi)$ is the effective frequency-dependent impedance and, the functions $P_S(\omega)$ and $P_D(\omega)$ represent the probability of photon absorption in the source and the drain resistors, respectively. These functions are defined as

$$P_l(\omega) = \int \frac{dt}{2\pi} e^{i\omega t} e^{-J_l(t)}, \quad (6)$$

here $l = S, D$ and J_l is the phase-phase correlation function given by [12]:

$$J_l(\omega) = \frac{4e^2 R_l}{\pi \hbar} \int_0^\infty d\omega' \frac{\coth \frac{\hbar \omega'}{2k_B T_l} (1 - \cos \omega' t) - i \sin \omega' t}{\omega (1 + \omega'^2 (R_S + R_D)^2 C_J^2)}. \quad (7)$$

The effective impedance $\tilde{Z}(\omega, \Phi)$ is defined as

$$\frac{1}{\tilde{Z}(\omega, \Phi)} = \frac{\pi I_c^2}{2\hbar \omega} [P(\omega) - P(-\omega) - i(P(\omega) + P(-\omega) - 2P(0)) \tan \frac{\pi(R_S + R_D)}{R_Q}], \quad (8)$$

where $P(\omega)$ is the P -function of the effective environment defined by the convolution of the $P(E)$ -function of the two resistors,

$$P(\omega) = \int d\omega' P_S(\omega - \omega') P_D(\omega'). \quad (9)$$

Supplemental information: Bolometric detection of coherent Josephson coupling in a highly dissipative environment

Diego Subero,^{1,*} Olivier Maillet,^{1,2,†} Dmitry S. Golubev,¹ George Thomas,¹ Joonas T. Peltonen,¹ Bayan Karimi,^{1,3} Marco Marín-Suárez,¹ Alfredo Levy Yeyati,⁴ Rafael Sánchez,⁴ Sunghun Park,⁴ and Jukka P. Pekola¹

¹*PICO Group, QTF Centre of Excellence, Department of Applied Physics, Aalto University School of Science, P.O. Box 13500, 0076 Aalto, Finland*

²*Université Paris-Saclay, CEA, CNRS, SPEC, 91191 Gif-sur-Yvette, France*

³*QTF Centre of Excellence, Department of Physics, Faculty of Science, University of Helsinki, 00014 Helsinki, Finland*

⁴*Departamento de Física Teórica de la Materia Condensada, Condensed Matter Physics Center (IFIMAC) and Instituto Nicolás Cabrera, Universidad Autónoma de Madrid, 28049 Madrid, Spain*

S1. CURRENT-VOLTAGE CHARACTERISTIC OF THE REPLICA SAMPLE

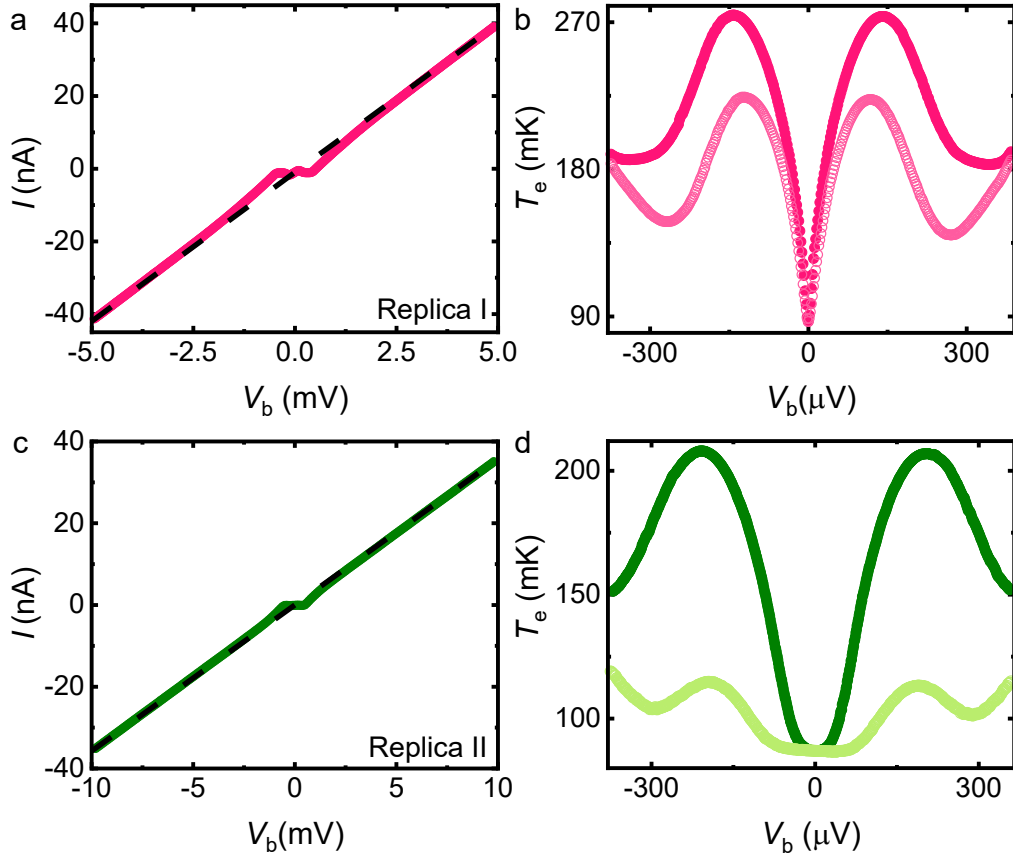


FIG. S1. a, c.- Current-voltage characteristic at large voltage bias of the Replica I and Replica II. The dashed black line is the linear fit. b, d.- Bias dependence of the temperature resistors in the low voltage bias regime at two magnetic flux values $\Phi = 0$ (solid circles) and $\Phi = \Phi_0/2$ (open circles), obtained from Eq. S4.

The quasiparticle tunnel resistance of the SQUID R_J and the superconducting gap were obtained from standard current-voltage measurements as depicted in Figs. S1a and S1c. The total resistance in series $R_T = R_S + R_D + R_J$ of the Replica was obtained by a linear fit, dashed black line in Figs. S1a and S1c. These resistances were: 122 k Ω for

Replica I and 280 k Ω for Replica II. Source and drain resistance were independently measured (see Fig. S2b) on-chip in a Cr-strip having the same size as those placed in the main and Replica sample and evaporated with the same target to be $R_S = R_D = 11$ k Ω . The electronic setup to measure this resistance is shown in Fig. S2a. Therefore, the resistance R_J was determined by subtracting from R_T the source R_S and drain R_D resistance values. Additionally, the superconducting gap was measured to be $\Delta = 200$ μ eV. Thus, the Josephson energy is calculated using the Ambegaokar-Baratoff relation $E_J = \Phi_0 \Delta / 4eR_J$. The single charging energy of the junction $E_C = e^2 / 2C_J$ is extracted from the current-voltage at a low bias, as explained in the main text, from which we estimate the SQUID capacitance to be 1.2 fF for Replica I and 0.7 fF for Replica II.

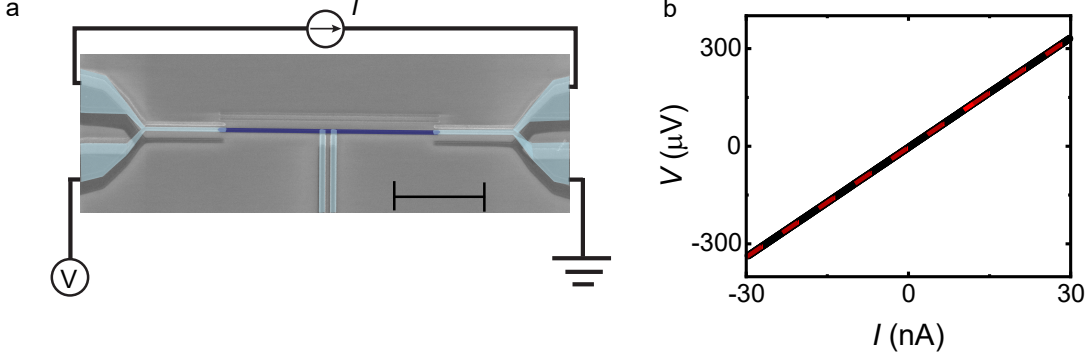


FIG. S2. a.- Colored scanning electron micrograph (scale bar: 5 μ m) highlighting the thin chromium normal metal (blue), with the schematics of the IV measurement. b.- Current-voltage curve measured at a phonon temperature of $T_0 = 87$ mK. The dashed line is the linear fit with a resistance value of $R = 11$ k Ω .

S2. JOSEPHSON CURRENT OF A SMALL JUNCTION EMBEDDED IN AN ELECTROMAGNETIC ENVIRONMENT

It is well established that the finite voltage bias current-voltage characteristic of a Josephson junction with a small critical current embedded in an electromagnetic environment at low bias is written as [S1, S2],

$$I = \frac{\pi e E_J^2(\Phi)}{\hbar} [P(2eV) - P(-2eV)], \quad (S1)$$

where $P(E)$ is the probability function that describes the energy exchange in the inelastic Cooper pair tunneling with the environment. This probability density is given by

$$P(E) = \frac{1}{2\pi\hbar} \int e^{iEt} \langle e^{i\hat{\varphi}(t)} e^{-i\hat{\varphi}(0)} \rangle = \frac{1}{2\pi\hbar} \int dt e^{i\frac{Et}{\hbar} - J(t)}, \quad (S2)$$

where

$$J(t) = \frac{4e^2}{\pi\hbar} \int_0^\infty d\omega \operatorname{Re}[Z_T(\omega)] \left[\coth \frac{\hbar\omega}{2k_B T(V_b)} \frac{1 - \cos \omega t}{\omega} + i \frac{\sin \omega t}{\omega} \right], \quad (S3)$$

is the phase-phase correlation function. Here, $Z_T(\omega)$ and $T(V)$ are the impedance seen by the junction and the bias voltage dependent temperature of the resistors. The latter is modeled in the usual way,

$$T(V) = \left[T_0^6 + \frac{IV_b}{2\Sigma\Omega} \right]^{1/6}, \quad (S4)$$

and its behavior is shown in Figs. S1b and S1d. Here, T_0 is the phonon temperature, $\Sigma = 12 \times 10^9$ WK $^{-6}$ m $^{-3}$ is the electron-phonon constant of the normal metal, and $\Omega = 1.4 \times 10^{-20}$ m 3 is the volume of each resistor. Factor 2 in Eq. (S4) accounts for the two resistors surrounding the SQUID. The impedance $Z_T(\omega)$ is derived from the resistively

and, capacitively shunted junction (RCSJ) model,

$$Z_T(\omega) = \frac{1}{-i\omega C_J + (R_S + R_D)^{-1}}, \quad \text{Re}[Z_T(\omega)] = \frac{R_S + R_D}{1 + \omega^2 (R_S + R_D)^2 C_J^2}. \quad (\text{S5})$$

Note that the asymmetry of the critical current of the SQUID in Eq. (S1) is taken into account through the parameter d as [S3]

$$E_J(\Phi) = E_J(0) |\cos(\pi\Phi/\Phi_0)| \sqrt{1 + d^2 \tan^2(\pi\Phi/\Phi_0)}. \quad (\text{S6})$$

S3. HEAT CURRENT THROUGH A SQUID CONNECTED IN SERIES WITH RESISTORS BASED ON THE $P(E)$ -THEORY

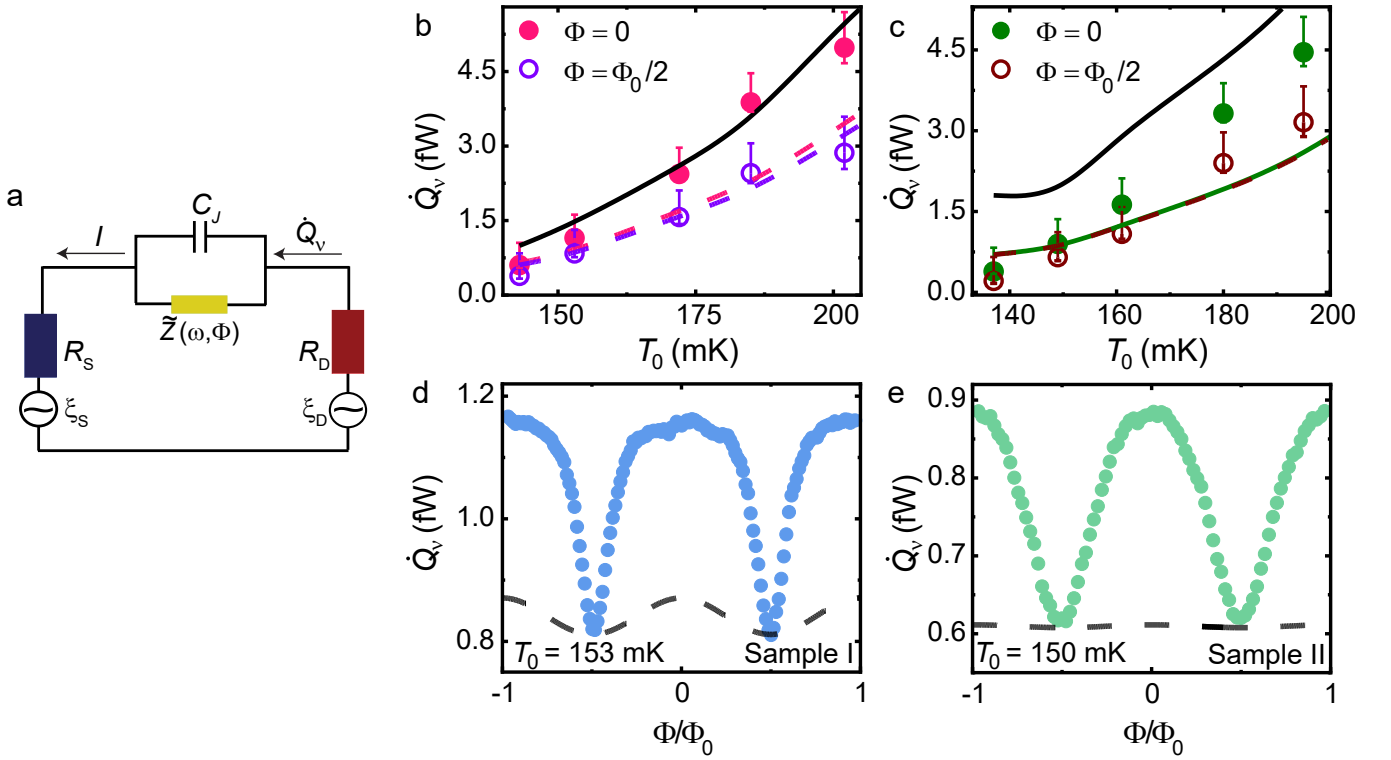


FIG. S3. a.-Schematic electric circuit of the device with an effective impedance $\tilde{Z}(\omega, \Phi)$ replacing the SQUID, in series with resistors. b, c, d, and e- Same data as shown in Fig. 4 of the main text. The solid line represents the power transmitted through a single channel at the quantum limit \dot{Q}_Q . The dashed lines are the theoretical results obtained from Eq. (S7) for the respective magnetic fluxes applied, with the circuit parameters obtained from fitting the IVC of the Replica samples in Fig. 2b and 2c, shown in the main text.

Here we consider the system shown in Fig. S3a. The photonic heat flux between the two resistors can be expressed as (see Ref. [S4])

$$\dot{Q}_v = \int_0^\infty \frac{d\omega}{2\pi} \hbar\omega \tau(\omega) \left[\frac{1}{e^{\hbar\omega/k_B T_D} - 1} - \frac{1}{e^{\hbar\omega/k_B T_S} - 1} \right] + \frac{\pi \hbar I_C^2}{4e^2} \int_{-\infty}^{+\infty} d\omega \omega P_D(\omega) P_S(-\omega). \quad (\text{S7})$$

This equation is similar to the one deduced by Thomas. *et.al.* [S4] for a SQUID connected in parallel with resistors. However, one should re-define the photon transmission probability $\tau(\omega)$ and the functions $P_S(\omega)$ and $P_D(\omega)$ for the

circuit shown in Fig. S3a. Namely, the transmission probability is expressed as

$$\tau(\omega) = \frac{4R_S R_D}{\left| R_S + R_D + \frac{1}{-i\omega C_J + \frac{1}{\tilde{Z}(\omega)}} \right|^2}, \quad (\text{S8})$$

where the effective impedance of the junction $\tilde{Z}(\omega)$ was already defined in the methods section of the main text (see Eq. (8)). To find the expressions for the functions $P_j(\omega)$ ($j = S, D$) we write down the classical equation of motion for the Josephson phase in the circuit of Fig. (a),

$$C \frac{\hbar \ddot{\varphi}}{2e} + \frac{1}{R_S + R_D} \frac{\hbar \dot{\varphi}}{2e} + I_C \sin \varphi = \frac{R_S \xi_S + R_D \xi_D}{R_S + R_D}. \quad (\text{S9})$$

In order to obtain the equation for the phase, we introduce the new effective resistances \mathcal{R}_S and \mathcal{R}_D such that the equation (S9) reads,

$$C_J \frac{\hbar \ddot{\varphi}}{2e} + \left(\frac{1}{\mathcal{R}_S} + \frac{1}{\mathcal{R}_D} \right) \frac{\hbar \dot{\varphi}}{2e} + I_C(\Phi) \sin \varphi = \eta_S + \eta_D \quad (\text{S10})$$

where

$$\mathcal{R}_j = \frac{(R_S + R_D)^2}{R_j}, \quad \eta_j = \frac{R_j \xi_j}{R_S + R_D}, \quad |\eta_j|_\omega^2 = \frac{R_j}{(R_S + R_D)^2} \omega \coth \frac{\hbar \omega}{2k_B T_j}, \quad (\text{S11})$$

Thus, for the circuit of Fig. S3a we find the functions $P_j(\omega)$ by replacing the expression (S11) in the Eqs. (S2, S3)

$$P_j(\omega) = \int \frac{dt}{2\pi} e^{i\omega t} e^{-J_j(t)}, \quad (\text{S12})$$

where

$$\begin{aligned} J_j(t) &= \frac{4e^2}{\pi \hbar} \int_0^\infty d\omega \frac{\coth \frac{\hbar \omega}{2k_B T_j} (1 - \cos \omega t) + i \sin \omega t}{\mathcal{R}_j \left| -i\omega C_J + \frac{1}{\mathcal{R}_S} + \frac{1}{\mathcal{R}_D} \right|^2} = \frac{4e^2}{\pi \hbar} \int_0^\infty d\omega \frac{R_j \left[\coth \frac{\hbar \omega}{2k_B T_j} (1 - \cos \omega t) + i \sin \omega t \right]}{(R_S + R_D)^2 \left| -i\omega C + \frac{R_S}{(R_S + R_D)^2} + \frac{R_D}{(R_S + R_D)^2} \right|^2} \\ &= \frac{4e^2}{\pi \hbar} \int_0^\infty d\omega \frac{R_j \left[\coth \frac{\hbar \omega}{2k_B T_j} (1 - \cos \omega t) + i \sin \omega t \right]}{(R_S + R_D)^2 \left| -i\omega C_J + \frac{1}{R_S + R_D} \right|^2} = \frac{4e^2 R_j}{\pi \hbar} \int_0^\infty d\omega \frac{\coth \frac{\hbar \omega}{2k_B T_j} (1 - \cos \omega t) + i \sin \omega t}{|1 - i\omega (R_S + R_D) C_J|^2}. \end{aligned} \quad (\text{S13})$$

* diego.suberorengel@aalto.fi

† olivier.maillet@cea.fr

[S1] Ingold, G.-L. & Nazarov, Y. V. Charge tunneling rates in ultrasmall junctions. (Springer) 21–107 (1992).

[S2] Saira, O. P. *et al.* Dispersive Thermometry with a Josephson Junction Coupled to a Resonator. *Phys. Rev. Applied.* **6**, 024005 (2016).

[S3] Ronzani, A. *et al.* Tunable photonic heat transport in a quantum heat valve. *Nat. Phys.* **14**, 991–995 (2018).

[S4] Thomas, G., Pekola, J. P. & Golubev, D. S. Photonic heat transport across a Josephson junction. *Phys. Rev. B.* **100**, 094508 (2019).